

## Polarization Estimation for Radio Pulsars

M. M. MCKINNON<sup>1</sup>

<sup>1</sup>*National Radio Astronomy Observatory, Socorro, NM 87801 USA*

### ABSTRACT

A number of polarization estimators have been developed for a variety of astrophysical applications to compensate measurements of linear polarization for a bias contributed by the instrumental noise. Most derivations of the estimators assume that the amplitude and orientation of the polarization vector are constant. This assumption generally is not valid for the radio emission from pulsars that fluctuates from pulse to pulse. The radio emission from pulsars, fast radio bursts, and magnetars can be elliptically polarized, and estimators of the total polarization and absolute value of the circular polarization are used in their observations. However, these estimators have not been formally developed to a level that is commensurate with those of linear polarization. Estimators are derived for circular, linear, and total polarization when the amplitude of the polarization vector is a constant or a random variable. Hybrid estimators are proposed for general application to pulsar polarization observations. They are shown to be more effective at removing instrumental noise than their commonly used counterparts.

### 1. INTRODUCTION

#### 1.1. *Classical Estimators of Linear Polarization*

Measurements of linear polarization contain a contribution from the instrumental noise, and a variety of methods have been developed to remove this instrumental bias from the measurements. The methods generally assume that the amplitude and orientation of the polarization vector are constant and the instrumental noise in each of the Stokes parameters  $Q$  and  $U$  is a Gaussian random variable (RV) such that the measured linear polarization ( $L = \sqrt{Q^2 + U^2}$ ) follows a Rice probability density function (pdf). Most methods use this pdf to derive a polarization estimator from which the intrinsic polarization may be inferred. Serkowski (1958) suggested that the measured polarization is equal to the mean of the pdf, while Wardle & Kronberg (1974) proposed that the measured polarization is equal to the mode of the pdf. Simmons & Stewart (1985) noted that the measured polarization could also be represented by the median and maximum likelihood (ML) of the pdf. They showed that all four estimators converge to the same result when the signal-to-noise ratio (SNR) in polarization is large. The relationship between the measured linear polarization,  $L_m$ , and the intrinsic polarization,  $\mu_q$ , in this SNR regime is  $L_m = \sqrt{\mu_q^2 + \sigma_n^2}$ , where  $\sigma_n$  is the magnitude of the instrumental noise. The convergence of the estimators arises from the Rice pdf evolving to a Gaussian pdf with a mean of  $\sqrt{\mu_q^2 + \sigma_n^2}$  and a standard deviation of  $\sigma_n$ , and because the mean, mode, median, and ML of a

Gaussian pdf are equal to one another. The asymptotic behavior of the estimators is often cited as the asymptotic, or AS, estimator (e.g., Plaszczyński et al., 2014; Montier et al., 2015).

### 1.2. Estimator Approximations

The mathematical expressions for the estimators can be complex and are not easily implemented in the data analysis. Instead, approximations are often made to the estimators using (e.g., Equation 16 of Simmons & Stewart 1985)

$$L_t = \begin{cases} (L_m^2 - K_a^2 \sigma_n^2)^{1/2} & \text{if } L_m > K_a \sigma_n \\ 0 & \text{otherwise,} \end{cases} \quad (1)$$

where  $L_t$  is an estimate of the true polarization and  $K_a$  is a threshold value determined by each estimator. The AS estimator is Equation 1 with  $K_a = 1$  and is equivalent to the approximation to Wardle & Kronberg's (1974) mode estimator. The pdf of the values of  $L_t$  resulting from the application of Equation 1 is discontinuous. It is comprised of a delta function at  $L_t = 0$ , owing to the cutoff at  $K_a \sigma_n$ , and a truncated Gaussian-like function (see, e.g., Figure 1 of Montier et al., 2015). The amplitude of the delta function increases with increasing  $K_a$ . If the value of  $K_a$  is too large, the measurements are overcompensated for instrumental noise, and the estimated value of the true polarization is systematically low. Conversely, if  $K_a$  is too small, the measurements are undercompensated for noise, and the polarization estimate is systematically high.

### 1.3. Estimator Residual Bias and Risk

Although the classical estimators are effective in removing most of the instrumental bias, a residual bias remains after their application. Simmons & Stewart (1985) compared the effectiveness of the mode, mean, median, and ML estimators by calculating their residual bias and risk, or standard error about the true polarization, from the pdf of  $L_t$ . The residual bias,  $B$ , and risk,  $R$ , are defined by

$$B = (\langle L_t \rangle - \mu_q) / \sigma_n, \quad (2)$$

$$R = \langle (L_t - \mu_q)^2 \rangle / \sigma_n^2, \quad (3)$$

where the angular brackets denote averages over the pdf. They found that the ML estimator produced the lowest residual bias at low SNR, and the mode estimator produced the lowest residual bias at intermediate to high SNR. Although not attainable in practice (Plaszczyński et al., 2014), a perfect estimator would produce a residual bias of zero and a risk of 1 for all values of  $\mu_q$ .

### 1.4. Additional Estimators

More sophisticated estimators have been developed to measure linear polarization, primarily for the cosmic microwave background radiation. Quinn (2012) proposed a Bayesian analysis for estimates of the polarization and its confidence intervals. Plaszczyński et al. (2014) developed a modified asymptotic (MAS) estimator that attenuates low SNR measurements, instead of setting all values below a certain threshold equal to zero, as in Equation 1. The pdf of  $L_t$  resulting from the MAS estimator is continuous. This estimator is essentially unbiased for SNRs greater than about 3. The classical estimators summarized in Simmons & Stewart (1985) assume the instrumental noise in each of the Stokes parameters  $Q$  and  $U$  is statistically independent and equal in magnitude. Plaszczyński

et al. (2014) and Montier et al. (2015) evaluate the case when the noise in  $Q$  and  $U$  is covariant and not equal.

Another estimator assumes that the measured polarization is the true polarization. Stewart & Simmons (1985) characterized this assumption as naive, a designation that has persisted in the literature to note that no attempt has been made to compensate the measurements for instrumental bias. The naive estimator is useful for demonstrating the improvements that can be made in bias removal with other estimators.

### 1.5. Pulsar Applications

For a number of reasons, additional development of the classical polarization estimators is needed for their application to radio pulsars, fast radio bursts (FRBs), and magnetars. First, in addition to reproducing the intrinsic polarization at high SNR, the estimators must minimize the contribution of the noise at low SNR so that the polarization off the pulse or burst is consistent with zero (e.g., Karastergiou & Johnson 2004). Everett & Weisberg (2001) developed a hybrid estimator, hereafter the EW estimator, for linear polarization that employs the AS estimator for bias compensation at high SNR and a cutoff of  $L_m = 1.57\sigma_n$  for bias compensation at low SNR. The EW estimator is commonly used in polarization observations of pulsars and FRBs (e.g., Johnston & Kerr 2018; Day et al., 2020; Serylak et al., 2021; Johnston et al., 2023; Posselt et al., 2023; Mckinven et al., 2023; Basu et al., 2024). Second, pulsar radio emission is generally elliptically polarized and frequently exhibits modes of orthogonal polarization (or OPMs; e.g., Manchester et al., 1975; Cordes et al., 1978; Backer & Rankin 1980; Stinebring et al., 1984). The superposition of incoherent OPMs can alter the polarization fraction across a pulsar’s average profile as the relative intensity of the modes changes with pulse longitude (McKinnon & Stinebring 1998, 2000). The polarization vectors of pulsars, FRBs, and magnetars can also trace arcs or great circles on the Poincaré sphere, respectively, as functions of pulse longitude (Dyks et al., 2021; Oswald et al., 2023b), time (Bera et al., 2025), and frequency (Lower et al., 2024). Their circular ( $V$ ), linear ( $L$ ), and total ( $P$ ) polarization can be low due to vector crossings of the sphere’s equator or poles, or to the simultaneous occurrence of incoherent OPMs of comparable intensity, making their measurement susceptible to the effects of instrumental noise. Therefore, accurate polarization measurements and applicable polarization estimators for  $V$  and  $P$ , in addition to  $L$ , are needed to test the viability of models developed for pulsar polarization (e.g., Dyks 2020; Dyks et al., 2021; Oswald et al., 2023b; McKinnon 2024). Karastergiou et al. (2003) and Karastergiou & Johnston (2004) developed a polarization estimator for the absolute value of circular polarization,  $|V|$ . Quinn (2014) derived the mode and ML estimators for  $P = \sqrt{Q^2 + U^2 + V^2}$ , and showed that measured values of  $P$  vary as  $P_m = \sqrt{\mu_p^2 + 2\sigma_n^2}$  at high SNR. Apart from these two examples, estimators for  $|V|$  and  $P$  have yet to be developed to a level that is commensurate with those of  $L$ . Finally, the assumption that the amplitude of a polarization vector is constant generally is not valid for radio pulsars, because the emission’s total intensity and polarization at a particular pulse longitude fluctuate from pulse to pulse. The modulation index of the total intensity, the ratio of its standard deviation to its mean, is indicative of the emission’s heavy modulation. For example, the 1352 MHz observations of Burke-Spolaor et al. (2012, their Figure 6) show that the minimum modulation index,  $\beta$ , observed across pulse profiles lies in the range of about  $0.1 < \beta < 2$  with a median value of  $\beta \simeq 1$  (see also Weltevedre et al., 2006, 2007). The modulation of the polarization is likely comparable to that of the total intensity. The pdf of the total intensity can range from

Gaussian at  $\beta < 0.2$  (e.g., McKinnon 2004), to exponential at  $\beta = 1$ , and log-normal for larger values of  $\beta$  (e.g., Cairns et al., 2001, 2004).

The fluctuations in polarized intensity raise a number of related questions regarding polarization estimation. Are the estimators derived from the assumption of a polarization vector with constant amplitude applicable to a vector with randomly varying amplitude? Must polarization estimators be customized to the statistical character of the polarization fluctuations? Can a single estimator for a specific polarization ( $|V|$ ,  $L$ , or  $P$ ) be developed for general use, regardless of the statistical character of the fluctuations? The purpose of this paper is to address these questions by deriving and comparing polarization estimators for  $|V|$ ,  $L$ , and  $P$  when the amplitude of the polarization vector is constant or random. An overarching goal of the paper is to improve estimators that are commonly used for pulsar polarization observations.

The paper is organized as follows. In Section 2, mode, median, mean, and ML estimators are derived for  $|V|$  and  $P$  for the case when the amplitude of the polarization vector is constant. The derivations assume the instrumental noise in each of the Stokes parameters are independent, Gaussian RVs with equal magnitude. A general hybrid estimator for  $|V|$ ,  $L$ , and  $P$  that uses the EW estimator as a template is proposed. In Section 3, polarization estimators are derived for  $|V|$ ,  $L$ , and  $P$  when the amplitude of the polarization vector is a Gaussian or exponential RV. The parameterization of the hybrid estimators is optimized by minimizing their residual bias. In Section 4, the effectiveness of the hybrid estimators in removing the instrumental noise is compared with that of their commonly used counterparts. Summary comments are listed in Section 5. Appendix A lists the equations for estimators of  $P$  when the amplitude of a polarization vector is constant. Appendix B lists the equations for the estimators of  $|V|$ ,  $L$ , and  $P$  when the polarization fluctuations are Gaussian.

## 2. ESTIMATORS FOR A POLARIZATION VECTOR WITH CONSTANT AMPLITUDE

### 2.1. Circular Polarization Estimation

Polarization estimators and their threshold values are derived from the pdf of the measured amplitude of the polarization vector. When the intrinsic circular polarization,  $V$ , is constant at  $\mu_v$ , the pdf of the measured values of  $V$  is Gaussian with a mean of  $\mu_v$  and a standard deviation of  $\sigma_n$ . The pdf of the absolute value of  $V$  is the sum of two Gaussian functions (e.g., Equation 27 of McKinnon & Stinebring 1998):

$$f_{|V|}(z) = \frac{1}{\sigma_n \sqrt{2\pi}} \left\{ \exp \left[ -\frac{(z + \mu_v)^2}{2\sigma_n^2} \right] + \exp \left[ -\frac{(z - \mu_v)^2}{2\sigma_n^2} \right] \right\}, \quad z \geq 0. \quad (4)$$

Examples of  $f_{|V|}(z)$  are shown in the top panel of Figure 1 for different SNR values in intrinsic circular polarization,  $s = \mu_v/\sigma_n$ .

The mean estimator for  $|V|$  is the mean of  $f_{|V|}(z)$  (Serkowski 1958) and is given by (e.g., Equation 13 of McKinnon & Stinebring 1998; Equation 2 of Karastergiou & Johnston 2004)

$$\langle z \rangle = \sigma_n \sqrt{\frac{2}{\pi}} \exp \left( -\frac{\mu_v^2}{2\sigma_n^2} \right) + \mu_v \operatorname{erf} \left( \frac{\mu_v}{\sigma_n \sqrt{2}} \right), \quad (5)$$

where  $\operatorname{erf}(x)$  is the error function. The threshold value of the mean estimator is determined from  $\langle z \rangle$  when  $\mu_v = 0$  and is equal to  $K_s = \sqrt{2/\pi}$ .

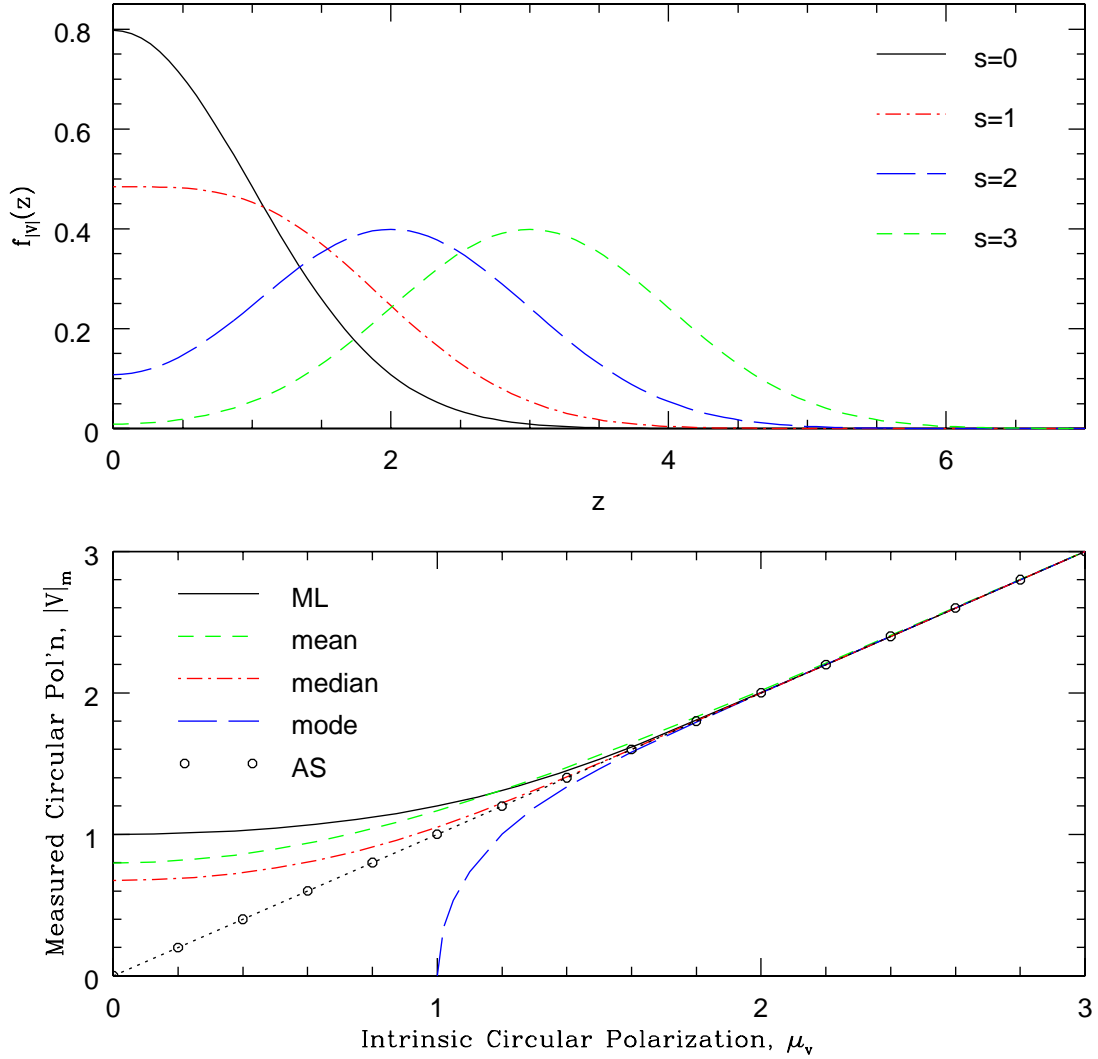


**Figure 1.** Probability density function (pdf) and polarization estimators for the absolute value of circular polarization when the amplitude of the polarization vector is constant. The top panel shows the pdf of  $|V|$  (Equation 4) for different values of SNR in intrinsic circular polarization,  $s = \mu_v/\sigma_n$ . The bottom panel compares the ML, mean, median, mode, and AS estimators for  $|V|$ . The dotted diagonal line denotes  $|V|_m = \mu_v$ . As with all figures, the magnitude of the instrumental noise used in the figure is  $\sigma_n = 1$ .

The mode estimator for  $|V|$  is derived by setting the derivative of  $f_{|V|}(z)$  with respect to  $z$  equal to zero (Wardle & Kronberg 1974). The mode estimator is the solution to

$$\frac{z}{\mu_v} = \tanh\left(\frac{z\mu_v}{\sigma_n^2}\right). \quad (6)$$

The mode of  $f_{|V|}(z)$  occurs at  $z = 0$  until  $\mu_v > \sigma_n$ . The threshold value of the mode estimator is  $K_w = 0$ .

The median estimator for  $|V|$  is the median,  $y$ , of  $f_{|V|}$  (Simmons & Stewart 1985) and satisfies the relation

$$1 = \operatorname{erf}\left(\frac{y + \mu_v}{\sigma_n \sqrt{2}}\right) + \operatorname{erf}\left(\frac{y - \mu_v}{\sigma_n \sqrt{2}}\right). \quad (7)$$

The threshold value for the median estimator is determined from Equation 7 when  $\mu_v = 0$ . It is equal to  $K_m = \operatorname{erf}^{-1}(1/2)\sqrt{2} = 0.6745$ , where  $\operatorname{erf}^{-1}(x)$  is the inverse error function.

The ML estimator is found by maximizing  $f_{|V|}(z)$  with respect to  $\mu_v$  (Simmons & Stewart 1985) and satisfies the relation

$$\frac{z}{\mu_v} = \coth\left(\frac{z\mu_v}{\sigma_n^2}\right). \quad (8)$$

The threshold value of the ML estimator is  $K_{ml} = 1$ . The threshold values of all four estimators are compiled in the second column of Table 1.

The estimators are compared in the bottom panel of Figure 1. All four estimators converge at an SNR of about  $s = 1.6$ , because the pdf of  $|V|$  approaches the Gaussian pdf of  $V$  at intermediate to high SNR. The panel shows that measurements of  $|V|$  are not biased by the instrumental noise at intermediate to high SNR. The asymptotic behavior of the estimators suggests they may be approximated by a simple detection threshold:

$$|V|_t = \begin{cases} |V|_m & \text{if } |V|_m > K_a \sigma_n \\ 0 & \text{otherwise.} \end{cases} \quad (9)$$

The approximation to the mode estimator (i.e., when  $K_a = K_w = 0$ ) is the AS estimator for  $|V|$  and is shown by the open circles in the bottom panel of the figure. Since it does not compensate measurements for instrumental noise, it is also the naive estimator for  $|V|$ .

The pdf of  $|V|_t$  is comprised of  $f_{|V|}(z)$  truncated on its low side at  $K_a \sigma_n$  and a delta function at  $z = 0$ . The residual bias and risk of the estimator approximations can be calculated analytically from the first and second moments of this pdf using their respective values of  $K_a$ . They are compared in Figure 2. The AS estimator quickly converges to zero bias but at the expense of a large bias and risk at small SNR. The other estimator approximations overshoot zero bias near  $s \simeq 1$ , but produce a lower bias than the AS estimator at  $s < 1$ . Similarly to Simmons & Stewart's (1985) finding for  $L$ , the approximation to the ML estimator for  $|V|$  produces the lowest bias at low SNR ( $s < 0.8$ ).

## 2.2. Total Polarization Estimation

When the amplitude of the total polarization vector is constant at  $\mu_p$ , the pdf of the measured vector amplitude is (e.g., Equation 11 of McKinnon 2003; Equation 24 of Quinn 2014)

$$f_P(r) = \frac{r}{\mu_p \sigma_n} \sqrt{\frac{2}{\pi}} \exp\left[-\frac{(r^2 + \mu_p^2)}{2\sigma_n^2}\right] \sinh\left(\frac{r\mu_p}{\sigma_n^2}\right). \quad (10)$$

Examples of  $f_P(r)$  are shown in the top panel of Figure 3 for different values of SNR in total polarization,  $s = \mu_p/\sigma_n$ . The pdf is Maxwell-Boltzmann when  $s = 0$ , and is Gaussian-like when  $s \gg 1$ . Quinn (2014) derived the mode and median estimators for  $P$ , and McKinnon (2003) calculated its mean estimator. All four estimators and their threshold values are compiled in Appendix A. The threshold values are also listed in the last column of Table 1. The estimators are shown in the

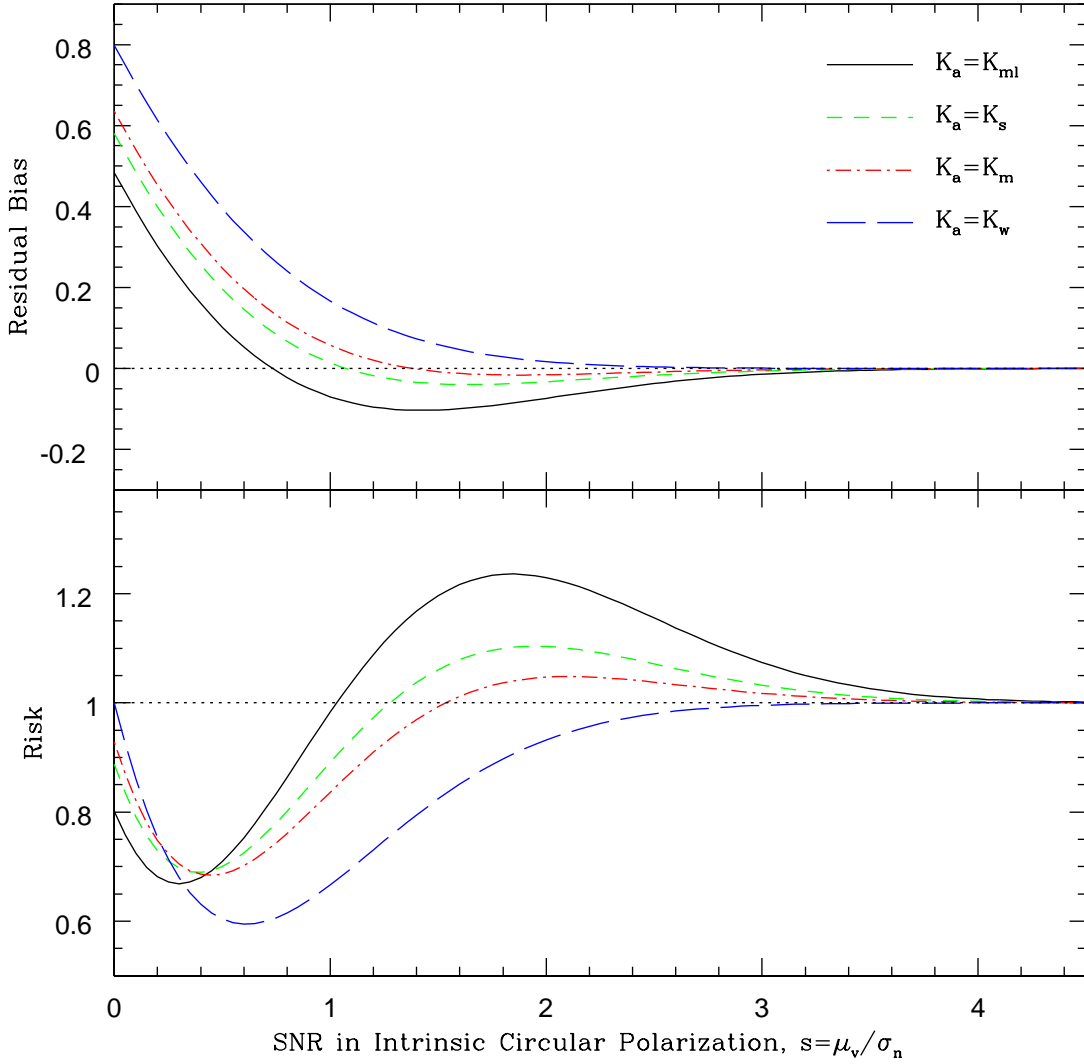


**Figure 2.** Residual bias and risk of the approximations to the circular polarization estimators. The top panel compares the residual bias of the approximations calculated from Equation 9 using different threshold values,  $K_a$ . The bottom panel compares the risk of the estimator approximations.

bottom panel of Figure 3. The measured polarization,  $P_m$ , predicted by all four estimators converges to  $P_m = \sqrt{\mu_p^2 + 2\sigma_n^2}$  at an SNR of about  $s = 2$  (Quinn 2014). The asymptotic behavior of  $P_m$  is due to  $f_P(r)$  evolving to a Gaussian with a mean of  $\sqrt{\mu_p^2 + 2\sigma_n^2}$  and a standard deviation of  $\sigma_n$ . The AS estimator for  $P$  is then given by Equation 1 with  $L$  replaced by  $P$  and with  $K_a = \sqrt{2}$ . It is shown by the open circles in the bottom panel of Figure 3.

Trends in the asymptotic behavior and threshold values of the estimators are evident in their progression from  $|V|$  to  $L$  to  $P$ . For each polarization, all estimators converge to the same result at high SNR. The threshold values for the mode, median, mean, and ML estimators of  $|V|$ ,  $L$ , and  $P$  are compared in Table 1. The threshold values for  $L$  were derived by Simmons & Stewart (1985). The table entries are arranged such that the threshold values increase down and toward the right of the

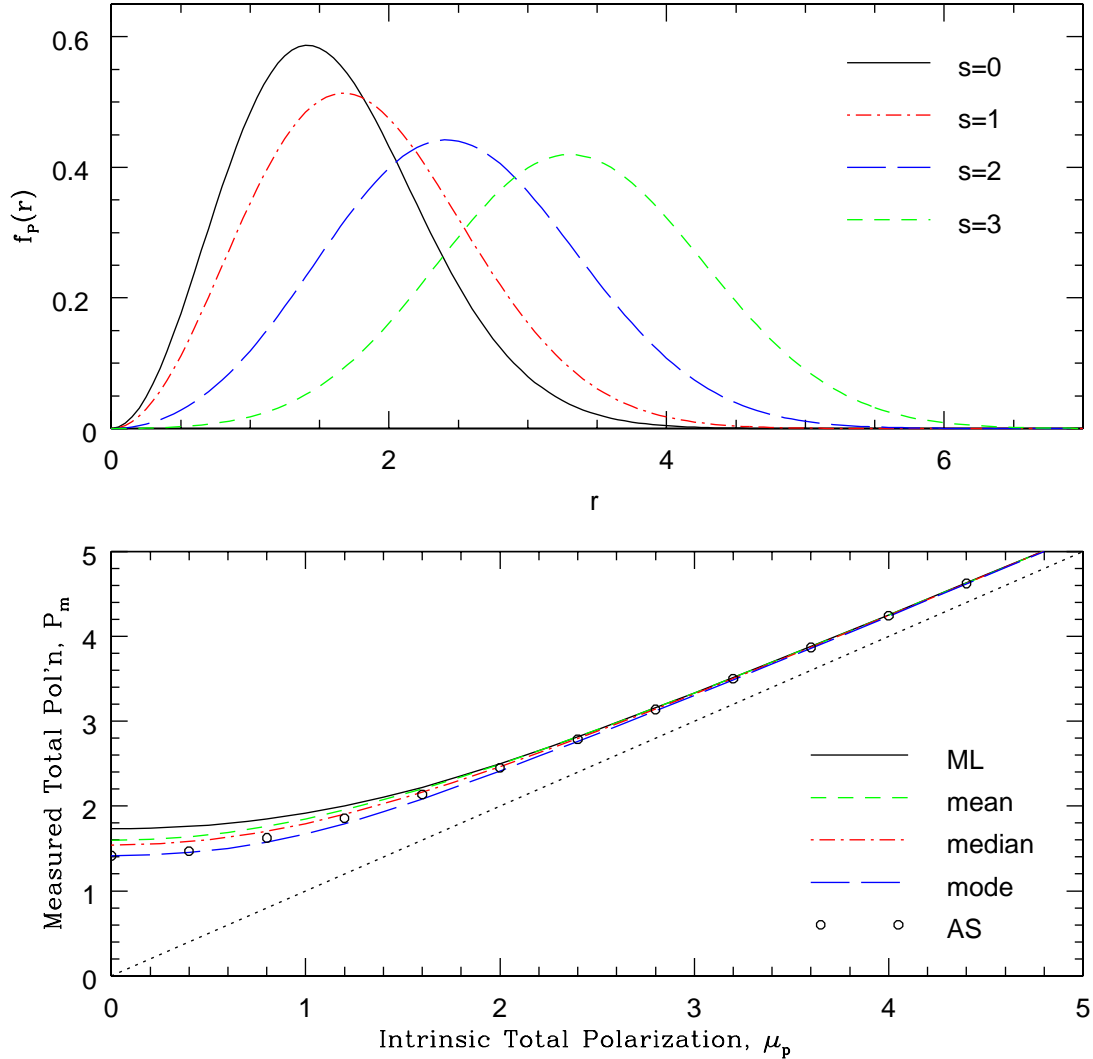


**Figure 3.** Probability density function (pdf) and polarization estimators for total polarization when the amplitude of the polarization vector is constant. The top panel shows the pdf of  $P$  (Equation 10) for different values of SNR in total polarization,  $s = \mu_p/\sigma_n$ . The bottom panel compares the ML, mean, median, mode, and AS estimators for  $P$ . The dotted diagonal line denotes  $P_m = \mu_p$ .

table. For a specific polarization, the mode threshold values are the smallest entries in the table, and the ML threshold values are the largest. For each estimator, the threshold for  $|V|$  is the smallest, and the  $P$  threshold is the largest. The last row of the table lists the number of dimensions,  $N$ , from the Poincaré sphere used in the derivation of the polarization amplitude pdfs. The threshold values of the mode estimator scale as  $\sqrt{(N-1)}$  (Quinn 2014), and the threshold values for the ML estimator scale as  $\sqrt{N}$ . These trends suggest that the basic form of the EW estimator can be generalized to a hybrid estimator for  $X = |V|$ ,  $L$ , or  $P$ :

$$X_t = \begin{cases} (X_m^2 - K_w^2 \sigma_n^2)^{1/2} & \text{if } X_m > K_c \sigma_n \\ 0 & \text{otherwise.} \end{cases} \quad (11)$$



**Table 1.** Estimator Threshold Values,  $K_a$ 

Polarization	Circular, $ V $	Linear, $L$	Total, $P$
Mode, $K_w$	0	1	$\sqrt{2}$
Median, $K_m$	$\text{erf}^{-1}(1/2)\sqrt{2}$	$\sqrt{2\ln(2)}$	1.5382
Mean, $K_s$	$\sqrt{2/\pi}$	$\sqrt{\pi/2}$	$\sqrt{8/\pi}$
ML, $K_{ml}$	1	$\sqrt{2}$	$\sqrt{3}$
Dimensions, $N$	1	2	3

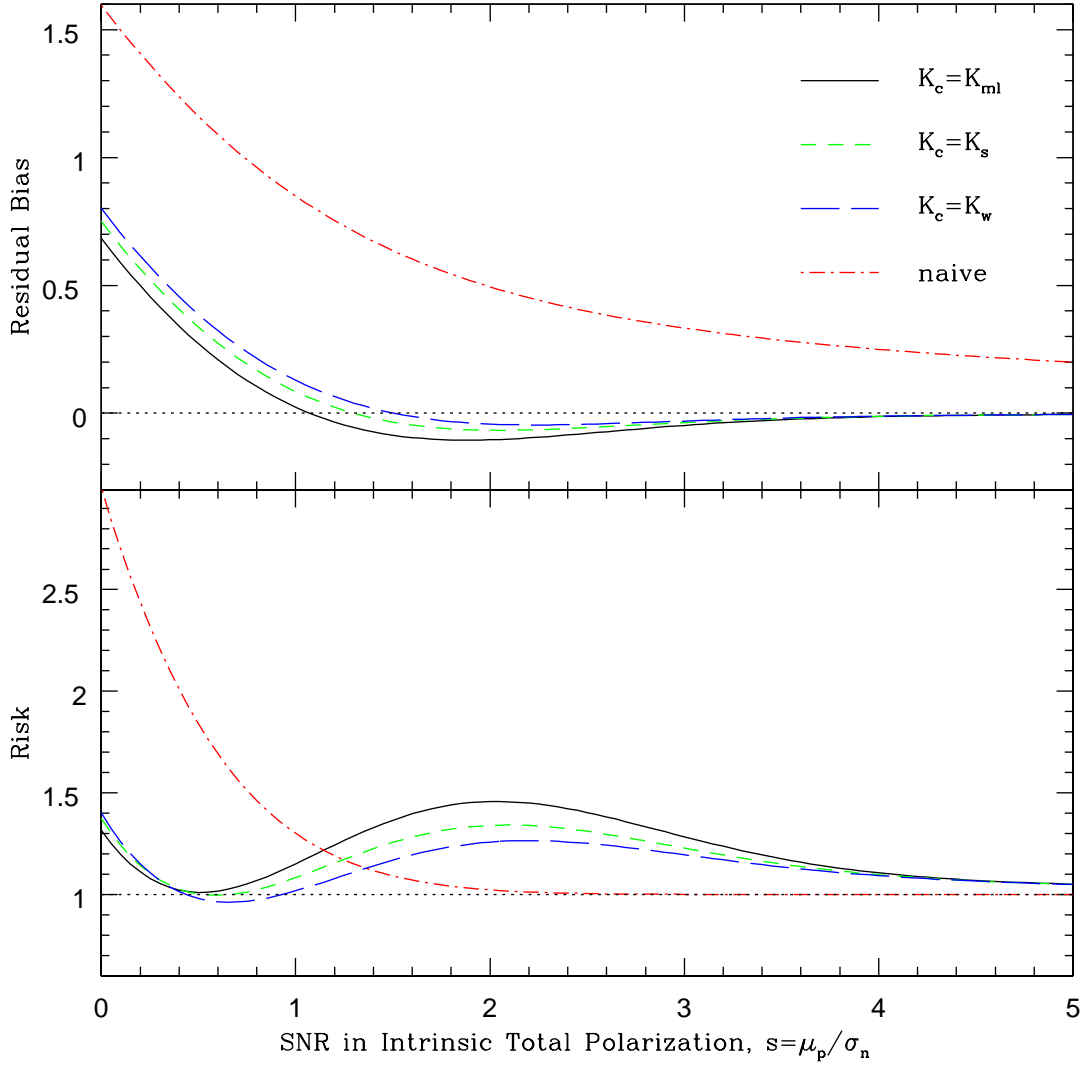
The constant  $K_w$  in Equation 11 is the relevant mode threshold from Table 1. It accounts for the noise contribution to the measured polarization at high SNR. The cutoff value,  $K_c$ , compensates the measured polarization for instrumental noise at low SNR and is constrained by  $K_c \geq K_w$  to ensure  $X_t$  is real. When  $X = |V|$ , the hybrid estimator becomes the estimator for  $|V|$  given by Equation 9, because  $K_w = 0$ . The hybrid estimator is the AS estimator when  $K_c = K_w$  and is the EW estimator when  $X = L$  and  $K_c = 1.57$ .

Figure 4 compares the residual bias and risk of the total polarization estimators calculated from Equation 11 using  $K_w = \sqrt{2}$  and different cutoff values,  $K_c$ , as listed in the figure. The bias and risk of the naive estimator for  $P$  were calculated analytically from the first and second moments of the pdf given by Equation 10. The bias and risk of the hybrid estimators were calculated numerically with Monte Carlo simulations. A simulation generated a half million ( $2^{19}$ ) samples each of the Stokes parameters  $Q$ ,  $U$ , and  $V$  at intrinsic polarization values ranging from  $\mu_p = 0$  to  $\mu_p = 5$  at intervals of  $\Delta\mu_p = 0.05$ . The hybrid estimator (Equation 11) was then applied to the individual values of  $P_m$  calculated from sets of  $Q$ ,  $U$ , and  $V$ . The residual bias and risk of the resulting values of  $P_t$  were calculated from the first and second moments of  $P_t$ . This procedure was repeated 64 times at each  $\mu_p$  interval to produce the mean bias and risk shown in the figure. The figure shows the significant improvements that can be made in bias removal with the hybrid estimator over the naive estimator. The bias of the naive estimator is approximately  $\sigma_n^2/\mu_p$  at high SNR ( $s > 3$ ). In contrast, the bias of the hybrid estimators converges to zero at  $s \simeq 4$ . The bias and risk of the naive estimator at low SNR ( $s < 1$ ) are much larger than their counterparts determined with the hybrid estimator. Of the hybrid estimators, the ML estimator ( $K_c = K_{ml}$ ) produces the lowest bias and risk at low SNR, but at the expense of slightly higher bias and risk in comparison to the other estimators at intermediate SNR ( $1 < s < 3$ ). The median hybrid estimator ( $K_c = K_m$ ) is not shown in the figure. It produces a bias and risk that are intermediate to those produced by the mode and mean hybrid estimators.

### 3. FLUCTUATIONS IN POLARIZED INTENSITY

The procedure for deriving polarization estimators when the amplitude of the polarization vector fluctuates is generally identical to that for a vector with constant amplitude (Section 2). In the following analysis, the pdfs for  $|V|$ ,  $L$ , and  $P$  are derived assuming the fluctuations are along the polarization vector. The term ‘‘fluctuations’’ refers to those occurring from pulse to pulse at a particular pulse longitude, as opposed to variations in the average polarization across a pulse profile.

Cairns et al. (2001, 2004) showed that the intensity fluctuations at specific pulse longitudes of PSRs B0833-45, B0950+08, and B1641-45 generally follow a log-normal pdf, and McKinnon (2004)



**Figure 4.** Residual bias and risk of the naive and hybrid estimators for total polarization. The top panel compares the residual bias of the hybrid estimators calculated from Equation 11 using  $K_w = \sqrt{2}$  and cutoff values of  $K_c = K_{ml}$ ,  $K_s$ , and  $K_w$  for  $P$  from Table 1. The bottom panel compares the risk of the estimators.

showed the fluctuations near the pulse center of PSR B2020+28 follow a Gaussian pdf. Deriving analytical expressions for the polarizations' observed pdfs and their estimators from a pulsar-intrinsic, log-normal pdf is not straightforward (e.g., Karastergiou & Johnson 2004). However, analytical expressions for the pdfs and their estimators can be derived when the fluctuations are assumed to be Gaussian or exponential RVs. Three scenarios are investigated. The first scenario assumes the pulse-to-pulse fluctuations are Gaussian with a mean amplitude that is greater than the amplitude fluctuations. The second scenario also assumes the fluctuations are Gaussian, but with a mean amplitude that is equal to zero, in which case the polarized signal consists of fluctuations, only. This can occur in pulsars through the incoherent addition of OPMs having the same mean intensity (McKinnon 2006). The third scenario assumes the intrinsic polarization fluctuations are exponential.

Given the larger modulation index of exponential intensity fluctuations, which is consistent with the median value of  $\beta$  indicated by Burke-Spoloar et al. (2012), this scenario may be more representative of what is observed in pulsar radio emission than Gaussian intensity fluctuations.

### 3.1. Gaussian Fluctuations with Nonzero Mean

When the fluctuations in the Stokes parameter  $V$  are Gaussian with a mean of  $\mu_v$  and a standard deviation of  $\sigma_v = \rho_v \sigma_n$ , the pdf for  $|V|$  is given by Equation 4 with  $\sigma_n$  replaced by  $\sigma_n \sqrt{1 + \rho_v^2}$ . Similarly, the polarization estimators determined from the pdf are the solutions to Equations 5 - 8 with  $\sigma_n$  replaced by  $\sigma_n \sqrt{1 + \rho_v^2}$ . Example pdfs of  $|V|$  for different values of SNR in the mean polarization,  $s = \mu_v/\sigma_n$ , and a fixed value of  $\rho_v = 2$  are shown in Figure 5(a). The polarization estimators for  $|V|$  are shown in Figure 5(b).

Assuming the linear polarization is concentrated in the Stokes parameter  $Q$  and the fluctuations in  $Q$  are Gaussian with a mean of  $\mu_q$  and a standard deviation of  $\sigma_q = \rho_q \sigma_n$ , the joint probability density of the amplitude of the linear polarization vector and its position angle,  $\psi$ , is (Equation 33 of McKinnon 2003)

$$f(r, \psi) = \frac{r}{\sigma_n^2 \pi (1 + \rho_q^2)^{1/2}} \exp \left[ -\frac{\mu_q}{2\sigma_n^2 (1 + \rho_q^2)} \right] \exp \left\{ -\frac{r^2 [1 + \rho_q^2 \sin^2(2\psi)]}{2\sigma_n^2 (1 + \rho_q^2)} \right\} \exp \left[ \frac{r \mu_q \cos(2\psi)}{\sigma_n^2 (1 + \rho_q^2)} \right]. \quad (12)$$

The pdf for  $L$  can be found by numerically integrating Equation 12 over  $\psi$ . The polarization estimators for  $L$  can then be determined numerically from the resulting pdf. Example pdfs of  $L$  for different values of SNR in its mean polarization,  $s = \mu_q/\sigma_n$ , and a fixed value of  $\rho_q = 2$  are shown in Figure 5(c). The polarization estimators for  $L$  are shown in Figure 5(d).

When the fluctuations in total polarization are Gaussian with a mean of  $\mu_p$  and a standard deviation of  $\sigma_p = \rho_p \sigma_n$ , the pdf for  $P$  from Equation 5 of McKinnon (2006) is

$$f_P(r) = \frac{r}{2\rho_p \sigma_n^2} \exp \left( -\frac{r^2}{2\sigma_n^2} \right) \exp \left( -\frac{\mu_p^2}{2\rho_p^2 \sigma_n^2} \right) \{ \operatorname{erfi}[h_+(r)] - \operatorname{erfi}[h_-(r)] \}, \quad (13)$$

where  $\operatorname{erfi}(x) = (-i)\operatorname{erf}(ix)$  is the imaginary error function,  $i = \sqrt{-1}$ , and the functions  $h_{\pm}(r)$  are given by

$$h_{\pm}(r) = \frac{\mu_p \pm r \rho_p^2}{\rho_p \sigma_n \sqrt{2(1 + \rho_p^2)}}. \quad (14)$$

Example pdfs of  $P$  for different values of SNR in its mean polarization,  $s = \mu_p/\sigma_n$ , and a fixed value of  $\rho_p = 2$  are shown in Figure 5(e).

The mode estimator for  $P$  is the solution to

$$\frac{r \rho_p \sigma_n}{r^2 - \sigma_n^2} \sqrt{\frac{2}{\pi(1 + \rho_p^2)}} = \frac{\operatorname{erfi}[h_+(r)] - \operatorname{erfi}[h_-(r)]}{\exp[h_+^2(r)] + \exp[h_-^2(r)]}, \quad (15)$$

and the ML estimator satisfies the relation

$$\frac{\rho_p \sigma_n}{\mu_p} \sqrt{\frac{2}{\pi(1 + \rho_p^2)}} = \frac{\operatorname{erfi}[h_+(r)] - \operatorname{erfi}[h_-(r)]}{\exp[h_+^2(r)] - \exp[h_-^2(r)]}. \quad (16)$$

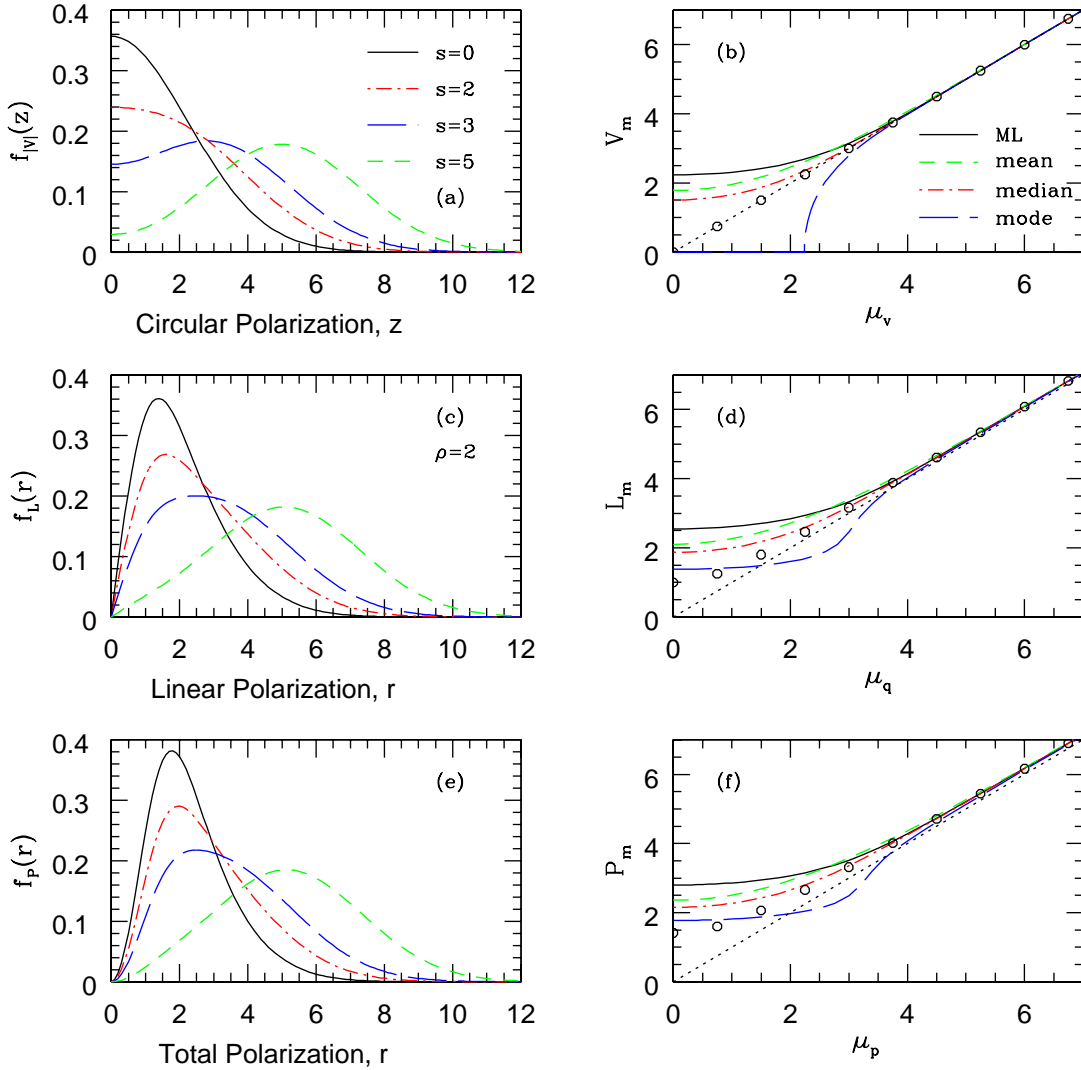


**Figure 5.** Example pdfs and polarization estimators when the polarization fluctuations are Gaussian with a nonzero mean. Panels (a), (c), and (e) on the left side of the figure show pdfs for  $|V|$ ,  $L$ , and  $P$ , respectively, for different values of SNR in intrinsic polarization,  $s = \mu/\sigma_n$ . Panels (b), (d), and (f) on the right side of the figure show the ML, mean, median, mode, and AS estimators for  $|V|$ ,  $L$ , and  $P$ , respectively. The open circles denote the AS estimator for each polarization. The ratio of the intrinsic polarization fluctuations to the instrumental noise in each panel is  $\rho = 2$ .

The mean and median estimators for  $P$  can be calculated numerically from the pdf given by Equation 13. The polarization estimators for  $P$  are shown in Figure 5(f).

Figure 5 shows that the pdfs for  $|V|$ ,  $L$ , and  $P$  and their estimators evolve in similar ways. As the SNR increases, the pdfs become Gaussian and the estimators approach their respective AS estimators. The estimator panels on the right side of the figure show the constant polarization,  $\mu$ , is the primary contributor to the measured polarization at high SNR, while the polarization fluctuations,  $\sigma$ , are the main contributor to the measured polarization at low SNR.

Consider a hypothetical radio source with Gaussian fluctuations in its total intensity and a constant polarization fraction. For the intrinsic total intensity to remain nonnegative, the mean intensity must exceed the fluctuations by about a factor of 5 ( $\mu \geq 5\sigma$  or  $\beta < 0.2$ ; McKinnon 2004). The same is true of the polarization since it is assumed to be a constant fraction of the total intensity. If the fluctuations are also greater than the instrumental noise ( $\rho > 1$ ), the measured polarization of the source will reside in the upper-right corner of the estimator panels in Figure 5. A conclusion that can be drawn from this scenario is the estimators derived for a source with a constant polarization amplitude can be used to estimate the mean polarization of a source with relatively small fluctuations in its polarization.

### 3.2. Gaussian Fluctuations with Zero Mean

The analysis heretofore has focused on an estimator's ability to replicate the constant component of the polarization. Now the focus shifts to testing an estimator's ability to replicate the polarization's fluctuating component.

When the fluctuations in the Stokes parameter  $V$  are Gaussian with a mean of  $\mu_v = 0$  and a standard deviation of  $\sigma_v = \rho_v \sigma_n$ , the pdf for  $|V|$  is given by Equation 4 with  $\mu_v$  set to zero and  $\sigma_n$  replaced by  $\sigma_n \sqrt{1 + \rho_v^2}$ . Example pdfs of  $|V|$  for different values of  $\rho_v$  are shown in Figure 6(a). The estimators derived from the pdf are listed in Appendix B. The ML estimator is the square root of the second moment of  $|V|$ , and the other estimators are proportional to it. The polarization estimators for  $|V|$  are shown in Figure 7(a).

When the fluctuations in the Stokes parameter  $Q$  are Gaussian with a mean of  $\mu_q = 0$ , the pdf of  $L$  is given by Equation 34 of McKinnon (2003):

$$f_L(r) = \frac{r}{\sigma_n^2(1 + \rho_q^2)^{1/2}} \exp \left[ -\frac{r^2(2 + \rho_q^2)}{4\sigma_n^2(1 + \rho_q^2)} \right] I_0 \left[ \frac{r^2 \rho_q^2}{4\sigma_n^2(1 + \rho_q^2)} \right] \quad (17)$$

The function  $I_0(x)$  in the pdf is the modified Bessel function of order zero. Example pdfs of  $L$  for different values of  $\rho_q$  are shown in Figure 6(c). The mean, mode, and ML estimators for  $L$  are listed in Appendix B. The median estimator can be calculated numerically from Equation 17. The polarization estimators for  $L$  are shown in Figure 7(c).

The pdf for Gaussian fluctuations only, in total polarization, is given by Equation 13 with  $\mu_p = 0$ :

$$f_P(r) = \frac{r}{\rho_p \sigma_n^2} \exp \left( -\frac{r^2}{2\sigma_n^2} \right) \operatorname{erfi} \left[ \frac{r \rho_p}{\sigma_n [2(1 + \rho_p^2)]^{1/2}} \right] \quad (18)$$

Example pdfs of  $P$  for different values of  $\rho_p$  are shown in Figure 6(e). The mean, mode, and ML estimators for  $P$  are listed in Appendix B. The median estimator can be calculated numerically from Equation 18. The polarization estimators for  $P$  are shown in Figure 7(e).

The pdfs for  $|V|$ ,  $L$ , and  $P$  on the left side of Figure 6 are generally similar to one another and evolve in similar ways. The same is true of their respective estimators, as shown on the left side of Figure 7. The pdfs are generally skewed half-Gaussians or asymmetric Gaussians with tails that extend as the fluctuations increase. Unlike the estimators for constant polarization that converge at high SNR, the estimators for fluctuating polarization diverge as the fluctuations increase. The divergence of the estimators is caused by the increased skewness of the pdfs. The quandary posed by the divergence of the estimators is which estimator, if any, can be used as a reliable indicator of the

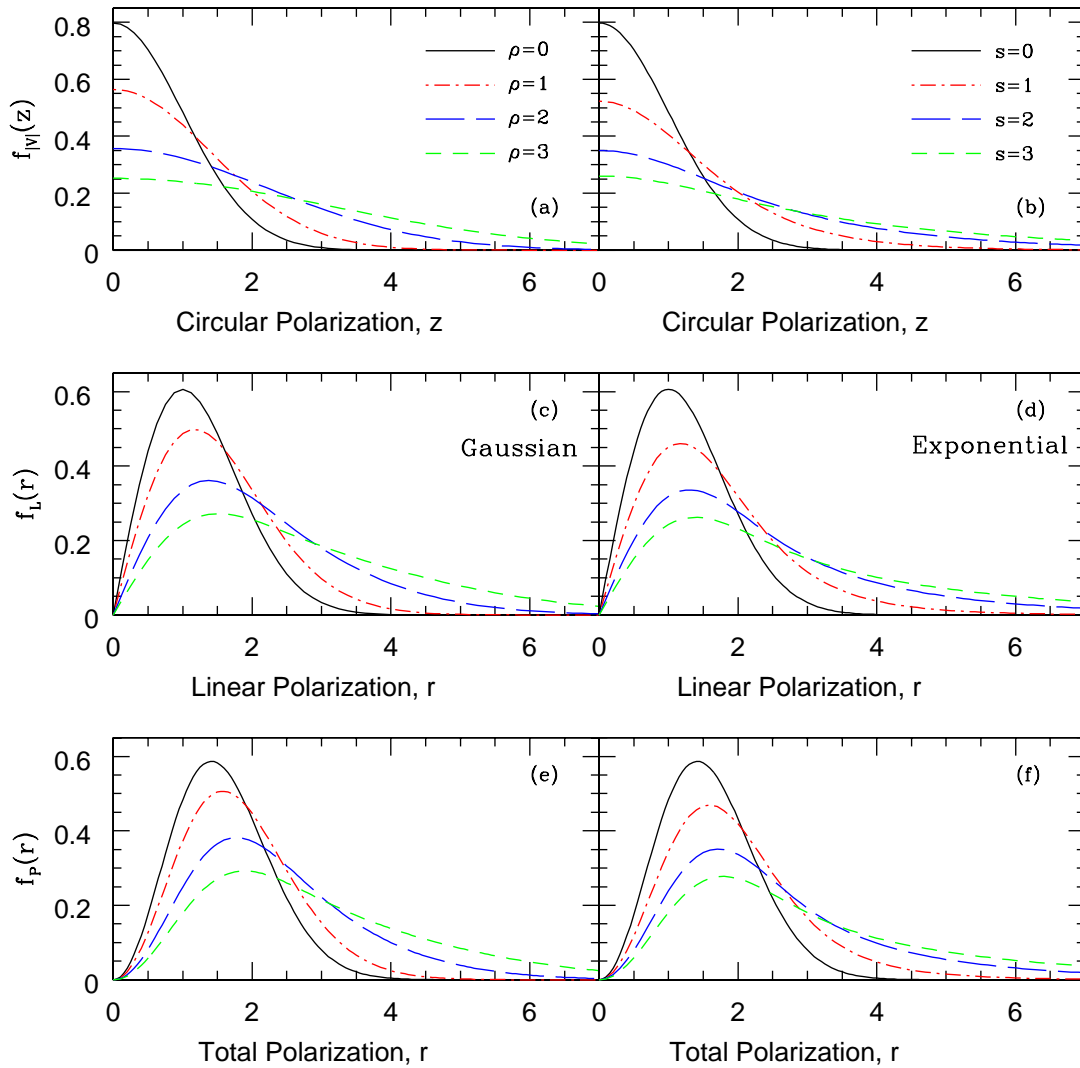


**Figure 6.** Comparison of pdfs for Gaussian and exponential fluctuations in polarization. Panels (a), (c), and (e) on the left side of the figure show the pdfs for  $|V|$ ,  $L$ , and  $P$ , respectively, when the polarization fluctuations are Gaussian. The example pdfs are shown for different values of the parameter  $\rho = \sigma/\sigma_n$  as annotated in panel (a). Panels (b), (d), and (f) on the right side of the figure show the pdfs for  $|V|$ ,  $L$ , and  $P$ , respectively, when the fluctuations are exponential. The pdfs are shown for different values of SNR in intrinsic polarization,  $s = \mu/\sigma_n$ , as annotated in panel (b).

intrinsic polarization fluctuations. The mode estimator is ineffective at predicting the polarization fluctuations, because it is essentially constant for all values of  $\rho$ . Owing to its large slope, the ML estimator is more sensitive to polarization fluctuations than the other estimators. As documented in Appendix B and as shown by the open triangles in panels (a), (c), and (e) of Figure 7, the ML estimator for  $|V|$ ,  $L$ , and  $P$  can be approximated by the square root of their second moments. The same cannot be said for the ML estimators derived for a polarization vector with constant amplitude

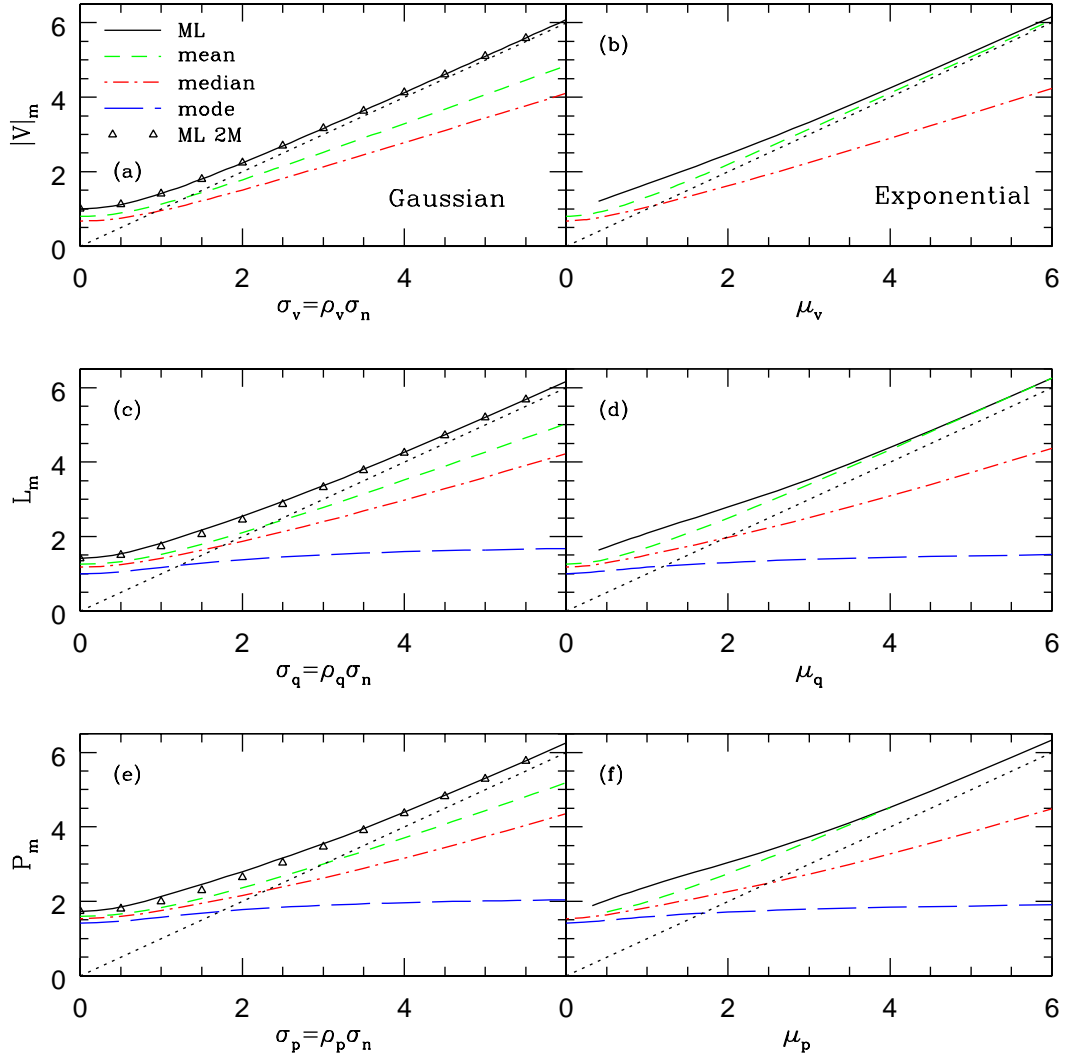


**Figure 7.** Comparison of the polarization estimators for Gaussian and exponential fluctuations in polarization. Panels (a), (c), and (e) on the left side of the figure show the ML, mean, median, and mode estimators for  $|V|$ ,  $L$ , and  $P$ , respectively, when the polarization fluctuations are Gaussian. The open triangles denote the approximations to the ML estimators determined by the polarization’s second moment (2M). Panels (b), (d), and (f) on the right side of the figure show the estimators for  $|V|$ ,  $L$ , and  $P$ , respectively, when the fluctuations are exponential. The mode estimators for  $|V|$  in panels (a) and (b) are always equal to zero.

(see Section 2). Practical estimators for polarization fluctuations are determined empirically from Equation 11 in Section 3.3.

### 3.3. Exponential Fluctuations

As mentioned in Section 1 and the introduction to Section 3, the intrinsic fluctuations in pulsar radio emission may be better represented by an exponential RV than a Gaussian RV. Additionally, a complete assessment of a Gaussian RV’s contribution to the measured polarization requires the independent determination of the two free parameters,  $\mu$  and  $\sigma$ , that characterize its pdf. Only

a single parameter must be determined in the case of an exponential RV, because the mean and standard deviation of its pdf are equal. The polarization pdfs and estimators arising from exponential fluctuations in the amplitude of a polarization vector are derived in the analysis that follows.

When the intrinsic fluctuations in circular polarization are exponential with a mean of  $\mu_v$ , the pdf of the observed  $V$  is the convolution of a truncated exponential with a zero mean Gaussian that represents the instrumental noise. The resulting pdf is given by Equation 4 of McKinnon (2014):

$$f_V(z) = \frac{1}{2\mu_v} \exp\left(\frac{\sigma_n^2}{2\mu_v^2}\right) \exp\left(-\frac{z}{\mu_v}\right) \left[1 + \operatorname{erf}\left(\frac{z - \sigma_n^2/\mu_v}{\sigma_n\sqrt{2}}\right)\right] \quad (19)$$

The pdf of  $|V|$  derived from Equation 19 is

$$f_{|V|}(z) = \frac{1}{2\mu_v} \exp\left(\frac{\sigma_n^2}{2\mu_v^2}\right) \left\{ \exp\left(-\frac{z}{\mu_v}\right) \left[1 + \operatorname{erf}\left(\frac{z - \sigma_n^2/\mu_v}{\sigma_n\sqrt{2}}\right)\right] + \exp\left(\frac{z}{\mu_v}\right) \operatorname{erfc}\left(\frac{z + \sigma_n^2/\mu_v}{\sigma_n\sqrt{2}}\right) \right\}, \quad (20)$$

where  $\operatorname{erfc}(z)$  is the complementary error function. Example pdfs of  $|V|$  for different values of  $s = \mu_v/\sigma_n$  are shown in Figure 6(b). The figure shows the mode of  $f_{|V|}$  always occurs at  $z = 0$ , regardless of the value of  $\mu_v$ . Therefore, the mode estimator for  $|V|$  is zero. The mean of  $f_{|V|}(z)$  is

$$\langle z \rangle = \sigma_n \sqrt{\frac{2}{\pi}} + \mu_v \exp\left(\frac{\sigma_n^2}{2\mu_v^2}\right) \operatorname{erfc}\left(\frac{\sigma_n}{\mu_v\sqrt{2}}\right). \quad (21)$$

The first term in Equation 21 implies that  $\langle z \rangle$  includes a constant contribution from the instrumental noise. However, the second term in the equation offsets this contribution as the SNR increases, such that the mean approaches  $\langle z \rangle \simeq \mu_v + \sigma_n^2/2\mu_v$  when  $\mu_v/\sigma_n \gg 1$ .

The median,  $y$ , of  $f_{|V|}(z)$  is the solution to

$$1 = 2\operatorname{erf}\left(\frac{y}{\sigma_n\sqrt{2}}\right) - \exp\left(\frac{\sigma_n^2}{2\mu_v^2}\right) \left\{ \exp\left(-\frac{y}{\mu_v}\right) \left[1 + \operatorname{erf}\left(\frac{y - \sigma_n^2/\mu_v}{\sigma_n\sqrt{2}}\right)\right] - \exp\left(\frac{y}{\mu_v}\right) \operatorname{erfc}\left(\frac{y + \sigma_n^2/\mu_v}{\sigma_n\sqrt{2}}\right) \right\}. \quad (22)$$

The ML estimator for  $|V|$  can be calculated numerically from Equation 20. The polarization estimators for  $|V|$  are shown in Figure 7(b).

Assuming the linear polarization is concentrated in the Stokes parameter  $Q$  and the fluctuations in  $Q$  are exponential with a mean of  $\mu_q$ , the joint probability density of the amplitude of the linear polarization vector and its position angle is

$$f(r, \psi) = \frac{r}{\mu_q \sigma_n \sqrt{2\pi}} \exp\left(-\frac{r^2}{2\sigma_n^2}\right) \exp\left\{\frac{[r \cos(2\psi) - \sigma_n^2/\mu_q]^2}{2\sigma_n^2}\right\} \left\{1 + \operatorname{erf}\left[\frac{r \cos(2\psi) - \sigma_n^2/\mu_q}{\sigma_n\sqrt{2}}\right]\right\}. \quad (23)$$

The pdf for  $L$  can be found by numerically integrating Equation 23 over  $\psi$ . The polarization estimators for  $L$  can then be determined numerically from the resulting pdf. Example pdfs of  $L$  for different values of  $s = \mu_q/\sigma_n$  are shown in Figure 6(d). The polarization estimators for  $L$  are shown in Figure 7(d).

When the intrinsic fluctuations in total polarization are exponential with a mean of  $\mu_p$ , the pdf for  $P$  is

$$f_P(r) = \frac{r}{\mu_p \sigma_n \sqrt{2}} \exp\left(-\frac{r^2}{2\sigma_n^2}\right) \int_{-w_+(r)}^{w_-(r)} \exp(x^2) [1 + \operatorname{erf}(x)] dx, \quad (24)$$



where the functions  $w_{\pm}(r)$  are given by

$$w_{\pm}(r) = \frac{r \pm \sigma_n^2/\mu_p}{\sigma_n\sqrt{2}}. \quad (25)$$

The estimators for  $P$  can be calculated numerically from the pdf given by Equation 24. Example pdfs of  $P$  for different values of  $s = \mu_p/\sigma_n$  are shown in Figure 6(f). The polarization estimators for  $P$  are shown in Figure 7(f).

Figure 6 shows that the pdfs derived for exponential fluctuations in a specific polarization ( $|V|$ ,  $L$ , or  $P$ ) are very similar to their counterparts derived for Gaussian fluctuations. The parameter  $\rho$  in the figure is a measure of the Gaussian fluctuations in polarization, while the parameter  $s$  is a measure of the exponential fluctuations. When the parameters are equal ( $\rho = s$ ), the respective pdfs are almost identical. The tails of the exponential pdfs are slightly more extended. Figure 7 shows that the estimators for Gaussian and exponential fluctuations in a specific polarization are also similar. The estimators for both generally diverge as the magnitude of the fluctuations increases, although the mean and ML estimators for exponential fluctuations approach one another at large values of  $\mu$ . For a specific polarization, the ML, median, and mode estimators produced by exponential fluctuations behave similarly and are roughly equal to their counterparts produced by Gaussian fluctuations. The similarities between specific estimators suggest they are somewhat insensitive to the statistical character of the fluctuations and that the same estimator can be used in both cases.

The analysis in Section 3.1 indicates that estimators for a constant vector amplitude can replicate the constant component of Gaussian amplitude fluctuations provided the constant component is larger than the fluctuating component. The analyses of Gaussian and exponential fluctuations in vector amplitude presented in Sections 3.2 and 3.3 suggest that estimators for a specific polarization may be insensitive to the statistical character of the fluctuations, although the best estimator for pure fluctuations in amplitude has yet to be determined. Acknowledging these traits, and with the goal of developing estimators for general use, the cutoff value,  $K_c$ , of the hybrid estimator proposed in Equation 11 was empirically optimized to minimize the residual bias produced by exponential fluctuations in vector amplitude. Potential candidates for  $K_c$  can be any one of the threshold values,  $K_a$ , listed in Table 1. However, as Everett & Weisberg (2001) have indicated, the optimum value of  $K_c$  is not restricted to values of  $K_a$ . The optimization trials began with  $K_c = K_s$  and  $K_c = K_{ml}$ , because the residual bias of  $|V|$  and  $P$  shown in Figures 2 and 4 demonstrates they are the most effective at removing instrumental bias at low SNR. Henceforth, the estimator with the optimum value of  $K_c$  is designated as the general purpose (GP) estimator.

The results of the optimization are shown in Figure 8. The top panel of the figure shows the residual bias in  $|V|$  for  $K_c = K_s$  and  $K_c = K_{ml}$  out to an SNR in circular polarization of  $s = 10$ . The estimator is always positively biased for  $K_c = K_s$ , but converges to zero bias at  $s \simeq 6$  when  $K_c = K_{ml} = 1$ . Values of  $K_c$  larger than 1 caused the estimator to overshoot zero bias, resulting in a negative bias at high SNR. Therefore, the GP estimator for  $|V|$  is its hybrid estimator (Equation 11) with  $K_c = 1$ . The middle panel of the figure compares the residual bias produced by different values of  $K_c$  used with the hybrid estimator for  $L$ . The values of  $K_c$  used in the optimization trials are annotated in the panel and include the EW estimator with  $K_c = 1.57$ . The panel shows the residual bias of the estimator with  $K_c = K_s$  and  $K_c = K_{ml}$  remains positive through  $s = 10$ . The residual bias of the EW estimator becomes slightly negative at  $s \simeq 3$ . The optimized cutoff value for the GP estimator of  $L$  was found to be  $K_c = 1.5$ , as shown by the red line in the panel. The bottom panel of the

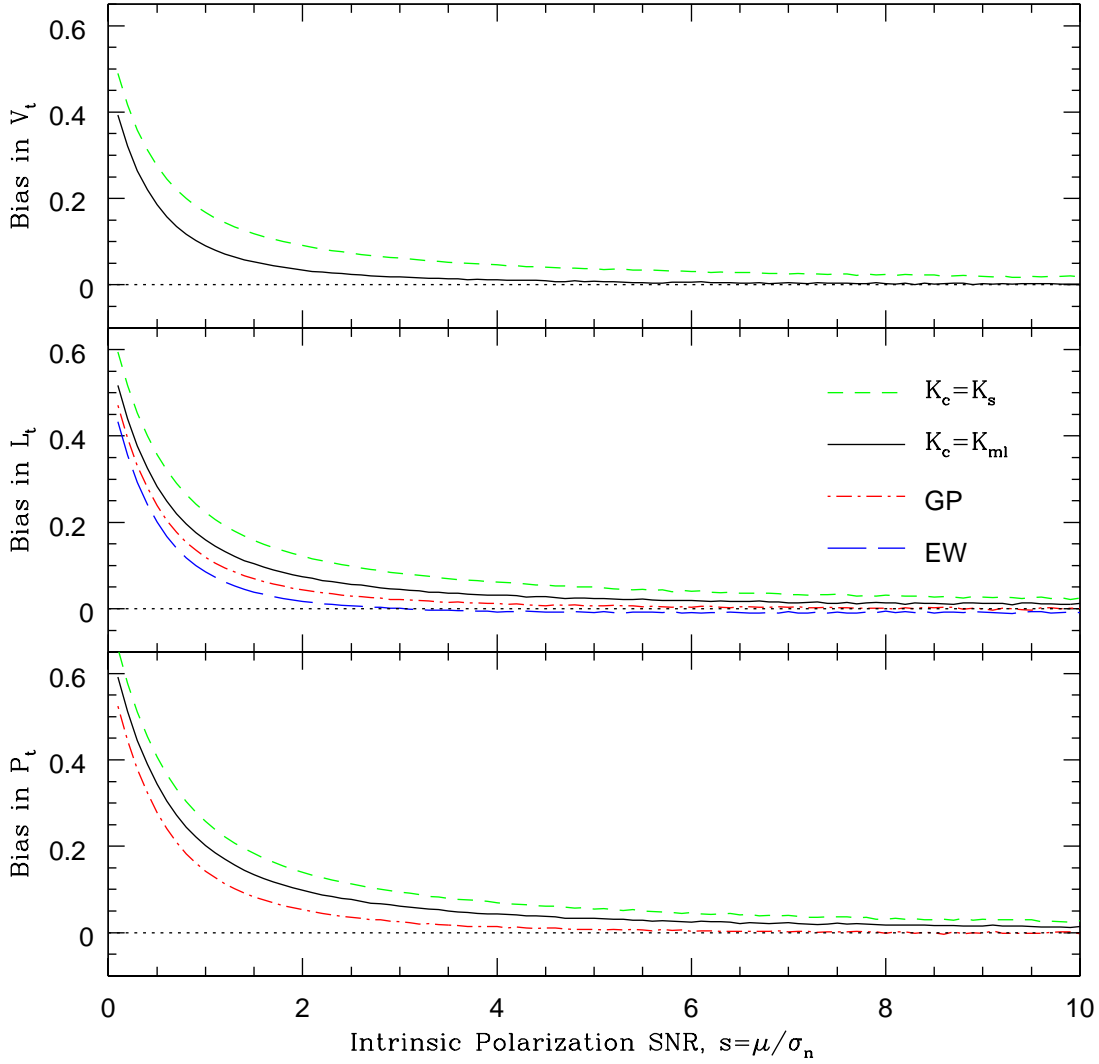


**Figure 8.** Residual bias of the hybrid estimator given by Equation 11 for  $|V|$  (top panel),  $L$  (middle panel), and  $P$  (bottom panel) when the fluctuations in polarization amplitude are exponential. The bias was calculated for different cutoff values,  $K_c$ , and is shown as a function of SNR in the relevant intrinsic polarization. The color code annotated in the middle panel of the figure applies to all three panels. The parameters  $K_w$  and  $K_c$  for the GP estimator are listed in Table 2. The GP estimator for  $|V|$  uses  $K_c = K_{ml}$ .

figure compares the residual bias produced by different values of  $K_c$  used with the hybrid estimator for  $P$ . The estimators using  $K_c = K_s$  and  $K_c = K_{ml}$  are again positively biased through  $s = 10$ . The optimized cutoff value for the GP estimator of  $P$  was found to be  $K_c = 1.85$ . The values of  $K_w$  and  $K_c$  determined for the GP estimators of  $|V|$ ,  $L$ , and  $P$  are summarized in Table 2. In each case, the optimum value of  $K_c$  is either equal to or slightly greater than  $K_{ml}$ . Although the parameters for the GP estimators were optimized assuming exponential fluctuations in the amplitude of the polarization vector, they are consistent with the parameters derived for a vector with constant amplitude. The parameters are consistent because the measured polarization approaches the intrinsic polarization at

**Table 2.** Parameters  $K_w$  and  $K_c$  for the General Purpose Estimators

Polarization	Circular, $ V $	Linear, $L$	Total, $P$
$K_w$	0	1	$\sqrt{2}$
$K_c$	1.0	1.5	1.85

high SNR and is dominated by the instrumental noise at low SNR in both scenarios. The statistics of the noise are independent of the intrinsic polarization fluctuations. Therefore, the GP estimators may be considered for general application to pulsar polarization observations.

#### 4. COMPARISONS WITH OTHER POLARIZATION ESTIMATORS

The estimator developed by Karastergiou et al. (2003) and Karastergiou & Johnston (2004) is often used to compensate measurements of  $|V|$  for instrumental noise (e.g., Johnston & Kerr 2018; Serylak et al., 2021; Oswald et al. 2023a; Posselt et al., 2023). The estimator is given by (e.g., Equation 6 of Posselt et al. 2023)

$$|V|_t = \begin{cases} |V|_m - \sigma_n \sqrt{2/\pi} & \text{if } |V|_m > \sigma_n \sqrt{2/\pi} \\ 0 & \text{otherwise.} \end{cases} \quad (26)$$

The estimator assumes the contribution of the instrumental noise to  $|V|_m$  is a constant and is essentially independent of the SNR in  $V$ . However, as shown in Figure 1, this assumption is not correct because  $|V|_m$  and  $\mu_v$  converge at an SNR of  $s \simeq 1.6$ . The estimator overcompensates  $|V|_m$  for noise such that the resulting values of  $|V|_t$  are systematically low by  $\sigma_n \sqrt{2/\pi}$  for  $s > 1.6$ . Values of  $|V|_t$  derived from Equation 26 have also been used to calculate the ellipticity angle of a polarization vector,  $\chi = 0.5 \arctan(|V|_t/L_t)$  (e.g., Oswald et al. 2023b). Since the estimator produces a value of  $|V|_t$  that is systematically low, the values of  $\chi$  calculated from it are also systematically low.

Tiburzi et al. (2013) use Equation 11 with  $X = |V|$ ,  $K_w = \sqrt{2/\pi}$ , and  $K_c = 2$  as an estimator for  $|V|$ . Similarly to Everett & Weisberg (2001), they do not mention why they chose their particular value of  $K_c$ . Their estimator generally overcompensates the measurements for instrumental noise and consequently produces estimates of  $|V|$  that are systematically low by approximately  $\sigma_n^2/(\pi\mu_v)$  at high SNR.

Figure 9 compares the residual bias and risk of the naive, MAS, AS, GP, and EW estimators for  $L$  when the amplitude of the polarization vector is constant. The residual bias and risk of the naive estimator shown in the figure were determined analytically from the first and second moments of the Rice pdf, and the bias and risk of the other estimators were calculated numerically with Monte Carlo simulations. The figure demonstrates the improvements that can be made in polarization estimation with the MAS, AS, GP and EW estimators over no noise compensation (the naive estimator). The MAS, AS, GP, and EW estimators have little to no residual bias for an SNR greater than  $s \simeq 3$ , because all four estimators have the same asymptotic behavior in the high SNR regime. A comparison between the residual bias of the AS, GP, and EW estimators illustrates the effect of their different cutoff values. The magnitude of the bias for the GP and EW estimators at low SNR is smaller than that for the AS estimator, because their larger cutoff values set a larger number of data points equal

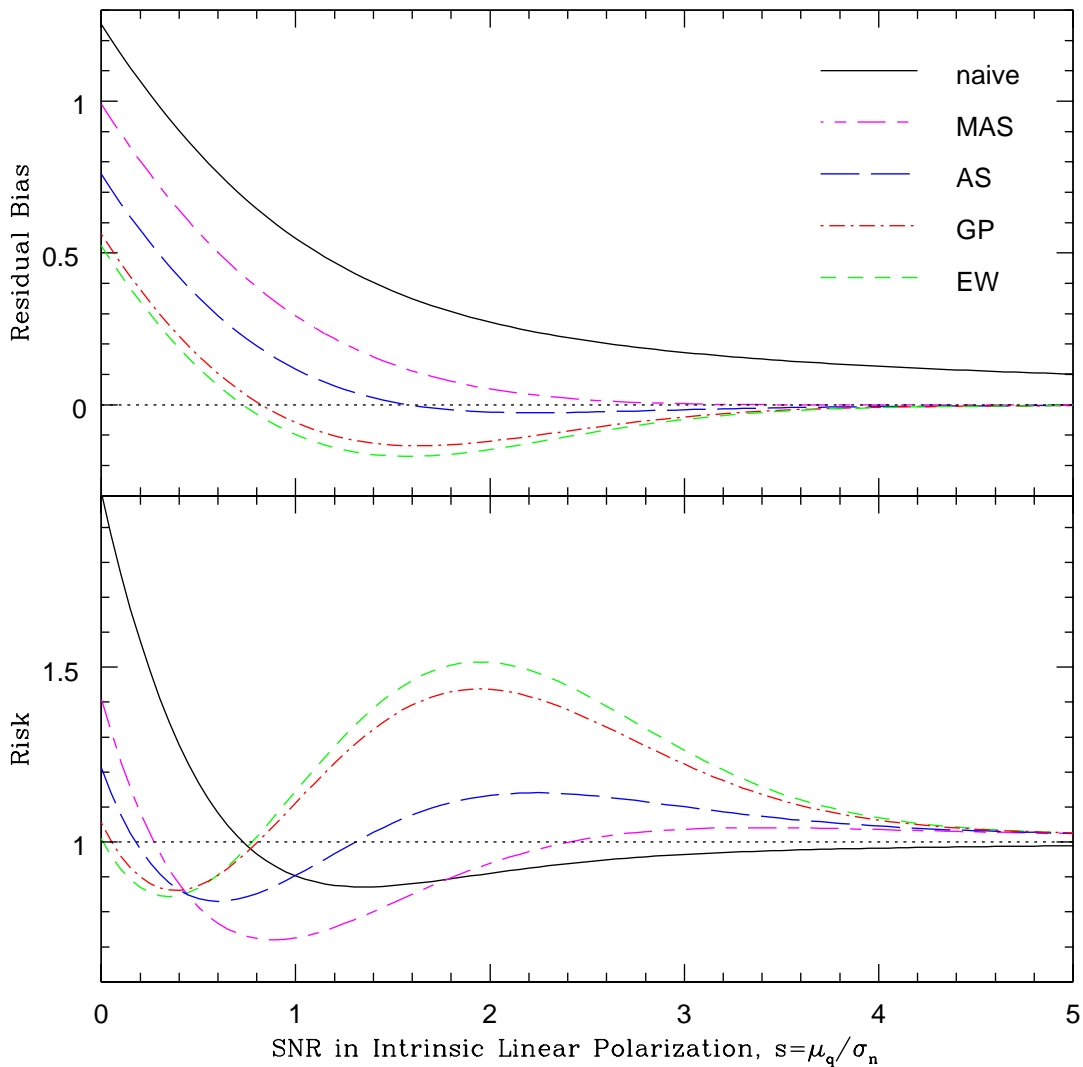


**Figure 9.** Comparison of the residual bias (top panel) and risk (bottom panel) of the naive, MAS, AS, GP, and EW estimators when the amplitude of the linear polarization vector is constant.

to zero. Therefore, the GP and EW estimators are more effective than the AS estimator at removing off-pulse instrumental noise. The trade-off in using the GP and EW estimators is their comparatively larger bias and risk at intermediate SNRs.

The MAS estimator for  $L$  is given by Equation 18 of Plaszczyński et al. (2014) and is replicated in Equation 27 below. As shown in Figure 9, it produces a residual bias that quickly converges to zero, and its risk is generally low in comparison to that of other estimators for  $s > 2$  (see also Figure 3 of Montier et al., 2015). However, the compromise made in using the MAS estimator is its large residual bias at low SNR where its magnitude is comparable to the instrumental noise. The relatively large bias is not unexpected, because the performance of both the AS and MAS estimators is optimized for intermediate to high SNR, as their names imply. When applied to exponential fluctuations in  $L$ , the MAS estimator returns a positive bias that is in excess of what is shown for the other estimators

in the middle panel of Figure 8 (e.g., the bias at  $s = 10$  is approximately 0.07). The MAS estimator can also be generalized for application to  $X = L$  or  $P$  with

$$X_t = X_m - \frac{K_w^2 \sigma_n^2}{2 X_m} \left[ 1 - \exp \left( -\lambda \frac{X_m^2}{\sigma_n^2} \right) \right]. \quad (27)$$

The constant  $K_w$  in Equation 27 is the relevant mode threshold from Table 1. The constant  $\lambda$  is determined empirically and is constrained by  $0 < \lambda \leq 2/K_w^2$  to ensure  $X_t \geq 0$ . Plaszczyński et al. (2014) found that  $\lambda = 1$  was optimum for measurements of  $L$ . Simulations of the MAS estimator’s residual bias indicate that a value of  $\lambda = 3/4$  is suitable for measurements of  $P$ . The MAS estimator could be applied to  $|V|$ , but it is equivalent to the naive estimator. Consequently, it is not an improvement upon the estimators given by Equations 9 and 11.

Different estimators have been used to compensate total polarization measurements for instrumental noise. For example, Oswald et al. (2023a) and Dial et al. (2025) apply the EW estimator for linear polarization to both  $L$  and  $P$ , and Dyks et al. (2021) apply Wardle & Kronberg’s (1974) mode estimator for  $L$  to both  $L$  and  $P$ . The application of estimators for  $L$  to measurements of  $P$  is not ideal, because the instrumental noise contributes more to  $P$  than it does to  $L$ . More specifically, the statistical properties of the noise for  $L$  and  $P$  are different: the noise in  $L$  follows a Rayleigh pdf, while the noise in  $P$  follows a Maxwell-Boltzmann pdf. The EW and mode estimators for  $L$  undercompensate measurements of  $P$  for instrumental noise such that the resulting values of  $P_t$  are systematically high by approximately  $\sigma_n^2/(2\mu_p)$  at high SNR.

Edwards & Stappers (2004) and MacQuart et al. (2012) note, though do not necessarily recommend, that a polarization’s second moment could be used as a polarization estimator. The attractive features of the second moment are it captures both the constant and fluctuating components of the polarization, its application is independent of the statistical character of the polarization fluctuations, and theoretically it can produce a zero residual bias. However, the second moment accurately measures the contribution of the instrumental noise only on average (MacQuart et al. 2012), and thus may be applicable only when a large number of data samples are used in computing the average polarization. The application of the second moment as a polarization estimator generally overcompensates the measurements for instrumental noise.

## 5. SUMMARY

Polarization estimators were derived for cases when the amplitude of a polarization vector is a constant or a RV. The residual bias and risk resulting from the application of approximations to the estimators were quantified. A hybrid estimator based on the EW estimator for linear polarization was proposed for general application to pulsar polarization observations. The parameterization of the hybrid estimators was optimized to minimize their residual bias. The optimized hybrid estimators were shown to be more effective at removing instrumental noise than their commonly used counterparts.

## ACKNOWLEDGMENTS

The National Radio Astronomy Observatory and Green Bank Observatory are facilities of the U.S. National Science Foundation operated under cooperative agreement by Associated Universities, Inc.

## APPENDIX

## A. TOTAL POLARIZATION ESTIMATORS

For a total polarization vector with constant amplitude, the mean estimator for  $P$  is given by Equation 12 of McKinnon (2003):

$$\langle r \rangle = \sigma_n \left[ \sqrt{\frac{2}{\pi}} \exp\left(-\frac{s^2}{2}\right) + \frac{s^2 + 1}{s} \operatorname{erf}\left(\frac{s}{\sqrt{2}}\right) \right], \quad (\text{A1})$$

where  $s = \mu_p/\sigma_n$  is the SNR in intrinsic total polarization. The mean approaches  $\langle r \rangle \simeq \mu_p + \sigma^2/\mu_p$  when  $s \gg 1$ . The threshold value of the mean estimator for  $P$  is  $K_s = \sqrt{8/\pi}$ .

The median estimator for  $P$  is the solution to

$$1 = \operatorname{erf}\left(\frac{y + \mu_p}{\sigma_n \sqrt{2}}\right) + \operatorname{erf}\left(\frac{y - \mu_p}{\sigma_n \sqrt{2}}\right) - \frac{\sigma_n}{\mu_p} \sqrt{\frac{8}{\pi}} \exp\left[-\frac{(y^2 + \mu_p^2)}{2\sigma_n^2}\right] \sinh\left(\frac{y\mu_p}{\sigma_n^2}\right). \quad (\text{A2})$$

The threshold value of the median estimator was calculated numerically, and is equal to  $K_m = 1.5382$ .

From Equation 25 of Quinn (2014), the mode estimator for  $P$  is the solution to

$$\frac{r\mu_p}{r^2 - \sigma_n^2} = \tanh\left(\frac{r\mu_p}{\sigma_n^2}\right). \quad (\text{A3})$$

The threshold value for the mode estimator is  $K_w = \sqrt{2}$ .

From Equation 26 of Quinn (2014), the ML estimator for  $P$  is the solution to

$$\frac{r\mu_p}{\mu_p^2 + \sigma_n^2} = \tanh\left(\frac{r\mu_p}{\sigma_n^2}\right). \quad (\text{A4})$$

The threshold value for the ML estimator is  $K_w = \sqrt{3}$ .

## B. ESTIMATORS FOR GAUSSIAN FLUCTUATIONS ONLY

B.1. *Circular Polarization*

When the fluctuations in the Stokes parameter  $V$  are Gaussian with a mean of  $\mu_v = 0$ , the mode of  $f_{|V|}(z)$  always occurs at  $z = 0$  (see Figure 6(a)). Therefore, the mode estimator for  $|V|$  is zero. The mean estimator for  $|V|$  is given by Equation 5 with  $\mu_v$  set to zero and with  $\sigma_n$  replaced by  $\sigma_n \sqrt{1 + \rho_v^2}$ :

$$\langle z \rangle = \sigma_n [2(1 + \rho_v^2)/\pi]^{1/2} \quad (\text{B5})$$

Similarly, the median estimator from Equation 7 is

$$y = \sigma_n \operatorname{erf}^{-1}(1/2) [2(1 + \rho_v^2)]^{1/2}. \quad (\text{B6})$$

Since  $\mu_v = 0$ , the estimators are tasked with quantifying the fluctuations in polarization amplitude. Therefore, the ML estimator is calculated by maximizing the pdf for  $|V|$  with respect to  $\rho_v$ . It is given by

$$z_{ml} = \sigma_n (1 + \rho_v^2)^{1/2} \quad (\text{B7})$$

and is equal to the square root of the second moment of  $|V|$  (see Figure 7(a)). The mean and median estimators are proportional to the ML estimator.

B.2. *Linear Polarization*

When the fluctuations in the Stokes parameter  $Q$  are Gaussian with a mean of  $\mu_q = 0$ , the mean estimator for  $L$  is the mean of Equation 17:

$$\langle r \rangle = \frac{2\sigma_n(1 + \rho_q^2)\sqrt{\pi}}{(2 + \rho_q^2)^{3/2}} {}_2F_1[3/4, 5/4; 1; \rho_q^4/(2 + \rho_q^2)^2] \quad (\text{B8})$$

The function  ${}_2F_1(a, b; c; z)$  in Equation B8 is the Gauss hypergeometric function with numerical parameters  $a$ ,  $b$ , and  $c$  and argument  $z$ . It is equal to one when  $z = 0$ .

The mode estimator for  $L$  is the solution to

$$\frac{r^2 \rho_q^2}{r^2(2 + \rho_q^2) - 2\sigma_n^2(1 + \rho_q^2)} = \frac{I_0[g(r)]}{I_1[g(r)]}, \quad (\text{B9})$$

where the argument of the Bessel functions has been abbreviated by

$$g(r) = \frac{r^2 \rho_q^2}{4\sigma_n^2(1 + \rho_q^2)}. \quad (\text{B10})$$

The ML estimator satisfies

$$\frac{r^2}{2\sigma_n^2(1 + \rho_q^2)} = \frac{I_0[g(r)]}{I_0[g(r)] + I_1[g(r)]}. \quad (\text{B11})$$

As shown in Figure 7(c), the ML estimator can be approximated by the square root of the second moment of  $L$ ,  $r = \sigma_n(2 + \rho_q^2)^{1/2}$ .

B.3. *Total Polarization*

When the fluctuations in total polarization are Gaussian with a mean of  $\mu_p = 0$ , the mean estimator for  $P$  is the mean of Equation 18:

$$\langle r \rangle = \frac{4\sigma_n}{[2\pi(1 + \rho_p^2)]^{1/2}} {}_2F_1[1/2, 2; 3/2; \rho_p^2/(1 + \rho_p^2)] \quad (\text{B12})$$

Alternatively, the mean of  $P$  can be written in terms of the inverse hyperbolic tangent,  $\text{arctanh}(x)$ :

$$\langle r \rangle = \sigma_n \sqrt{\frac{2}{\pi}} \left\{ (1 + \rho_p^2)^{1/2} + \frac{1}{\rho_p} \text{arctanh} \left[ \frac{\rho_p}{(1 + \rho_p^2)^{1/2}} \right] \right\}. \quad (\text{B13})$$

The mode polarization estimator satisfies the relation

$$\frac{r \rho_p \sigma_n}{r^2 - \sigma_n^2} \sqrt{\frac{2}{\pi(1 + \rho_p^2)}} = \text{erfi} \left[ \frac{r \rho_p}{\sigma_n \sqrt{2(1 + \rho_p^2)}} \right] \exp \left[ -\frac{r^2 \rho_p^2}{2\sigma_n^2(1 + \rho_p^2)} \right], \quad (\text{B14})$$

and the ML estimator is the solution to

$$\frac{r}{\sigma_n} \sqrt{\frac{2}{\pi}} \frac{\rho_p}{(1 + \rho_p^2)^{3/2}} = \text{erfi} \left[ \frac{r \rho_p}{\sigma_n \sqrt{2(1 + \rho_p^2)}} \right] \exp \left[ -\frac{r^2 \rho_p^2}{2\sigma_n^2(1 + \rho_p^2)} \right]. \quad (\text{B15})$$

As shown in Figure 7(e), the ML estimator can be approximated by the square root of the second moment of  $P$ ,  $r = \sigma_n(3 + \rho_p^2)^{1/2}$ .

## REFERENCES

- Bera, A., James, C., McKinnon, M. M., et al. 2025, ApJ, in press
- Burke-Spolaor, S., Johnston, S., Bailes, M., et al. 2012 MNRAS, 423, 1351
- Cairns, I. H., Johnston, S., & Das, P. 2001, ApJ, 563, L65
- Cairns, I. H., Johnston, S., & Das, P. 2004, MNRAS, 353, 270
- Cordes, J. M., Rankin, J., & Backer, D. C. 1978, ApJ, 223, 961
- Day, C. K., Deller, A. T., Shannon, R. M., et al. 2020, MNRAS, 497, 3335
- Dial, T., Deller, A. T., Uttarkar, P. A., et al., 2025, MNRAS, 536, 3220
- Dyks, J. 2020, MNRAS, 495, L118
- Dyks, J., Weltevrede, P., & Ilie, C. 2021, MNRAS, 501, 2156
- Edwards, R. T. & Stappers, B. W. 2004, A&A, 421, 681
- Everett, J. E. & Weisberg, J. M. 2001, ApJ, 553, 341
- Johnston, S. & Kerr, M., 2018, MNRAS, 474, 4629
- Johnston, S., Kramer, M., Karastergiou, A. et al. 2023, MNRAS, 520, 4801
- Karastergiou, A., Johnston, S., Mitra, D., et al. 2003, MNRAS, 344, L69
- Karastergiou, A. & Johnston, S., 2004, MNRAS, 352, 689
- Lower, M. E., Johnston, S., Lyutikov, M., et al., 2024, Nature, 8, 606
- MacQuart, J.-P., Ekers, R. D., Feain, I., & Johnston-Hollitt, M. 2012, ApJ, 750, 139
- Manchester, R. N., Taylor, J. H., & Huguenin, G. R. 1975, ApJ, 196, 83
- McKinnon, M. M. 2003, ApJS, 148, 519
- McKinnon, M. M. 2004, ApJ, 606, 1154
- McKinnon, M. M. 2006, ApJ, 645, 551
- McKinnon, M. M. 2014, PASP, 126, 476
- McKinnon, M. M. 2024, ApJ, 973, 35
- McKinnon, M. M. & Stinebring, D. R. 1998, ApJ, 502, 883
- McKinnon, M. M. & Stinebring, D. R. 2000, ApJ, 529, 435
- Mckinven, R., Gaensler, B. M., Michilli, D. et al. 2023, ApJ, 951, 82
- Montier, L., Plaszczyński, S., Levrier, F. et al., 2015, A&A, 574, A136
- Oswald, L. S., Johnston, S., Karastergiou, A., et al. 2023a, MNRAS, 520, 4961
- Oswald, L. S., Karastergiou, A., & Johnston, S. 2023b, MNRAS, 525, 840
- Plaszczyński, S., Montier, L., Levrier, F. et al. 2014, MNRAS, 439, 4048
- Posselt, B., Karastergiou, A., Johnston, S. et al. 2023, MNRAS, 520, 4582
- Quinn, J. L. 2012, A&A, 538, A65
- Quinn, J. L. 2014, A&A, 571, A89
- Serkowski, K. 1958, Acta Astron., 8, 135
- Serylak, M., Johnston, S., Kramer, M. et al., 2021, MNRAS, 505, 4483
- Simmons, J. F. L. & Stewart, B.G., 1985, A&A, 142, 100
- Stinebring, D. R., Cordes, J. M., Rankin, J. M., et al. 1984, ApJS, 55, 247
- Tiburzi, C., Johnston, S., Bailes, M. et al., 2013, MNRAS, 436, 3557
- Wardle, J. F. C. & Kronberg, P. P., 1974, ApJ, 194, 249
- Weltevrede, P., Edwards, R. T., & Stappers, B. W. 2006, A&A, 445, 243
- Weltevrede, P., Stappers, B. W., & Edwards, R. T. 2007, A&A, 469, 607